Chemical Physics Letters 827 (2023) 140712

Contents lists available at ScienceDirect

Chemical Physics Letters

journal homepage: www.elsevier.com/locate/cplett

N, S co-doped porous graphene-like carbon synthesized by a facile coal tar pitch-blowing strategy for high-performance supercapacitors

Gang Li [a], Shanshan Chen [b], Yonggang Wang [a], Gang Wang [b,*], Yuhan Wu [c,d,*], Yang Xu [e,*]

[a] School of Chemical and Environmental Engineering, China University of Mining and Technology, Beijing 100083, China
[b] College of Chemistry and Chemical Engineering, Shihezi University, Shihezi 832003, China
[c] School of Environmental and Chemical Engineering, Shenyang University of Technology, Shenyang 110870, China
[d] Key Laboratory of Advanced Energy Materials Chemistry (Ministry of Education), Nankai University, Tianjin 300071, China
[e] Department of Chemistry, University College London, London WC1H 0AJ, UK

ARTICLE INFO

Keywords:
Coal tar pitch
Heteroatom doping
Graphene-like carbon
Blowing strategy
Supercapacitor

ABSTRACT

Herein, coal tar pitch (CTP) derived nitrogen and sulfur co-doped porous graphene-like carbon (NSPC) is performed by an ammonium sulfate-assisted chemical blowing strategy. Afterward, NSPC was activated by KOH to form a-NSPC features a bubble-like structure with a thin porous shell and a well-balanced porous ratio. Serving as electrode materials for supercapacitors, the capacitance of a-NSPC was 368 F g^{-1} at 0.5 A g^{-1}. Meanwhile, the prepared materials exhibit excellent cycling stability after 10,000 cycles. This work may not only prepare superior electrode materials but also provide a feasible strategy for large-scale production of high-performance and low-cost electrode materials.

1. Introduction

Electrochemical energy storage technologies are a promising strategy to deal with the energy crisis. They enable the efficient use of renewable energy (e.g. wind, sunlight, and tides). Supercapacitors as a promising candidate by virtue of high-power density, rapid charge–discharge rate, and long-term cycle life have been employed as a power source in electric devices [1–3]. Nonetheless, to achieve large-scale applications, developing high-performance and low-cost electrode materials is still a great challenge.

Carbon materials have been widely used as electrode materials because of their merits of high electrical conductivity, superior stability, and low weight. Among various carbon materials, graphene holds great advantages [4]. However, its electrochemical performance is still unsatisfactory. For example, the reported specific capacitance is far below the theoretical value of 550 F g^{-1}. Porosification is a favorable option because porous graphene possesses a large surface area and short transport pathways, which are in favor of charge storage and charge transfer [5]. As for the production cost of graphene, it currently seems less competitive than commercial carbon materials. It is highly necessary to explore cheaper raw materials and manufacturing processes.

Due to reproducibility and environmental friendliness, many researchers pay attention to biomass as the precursor of carbon materials. In addition, biomass-derived carbon materials can readily inherit the unique structure, defects, and chemical composition of biomass precursors [6,7]. However, the uneven distribution of biomass limits its industrial applications. Coal tar pitch (CTP) as a byproduct of coal tar distillation can be obtained continuously and meanwhile, features a high carbon content and low cost. Meanwhile, it contains a large number of polycyclic aromatic hydrocarbons that consist of sp^2-hybridized carbon and has a narrow size distribution. These properties make it possible to directly synthesize porous graphene from CTP [8]. However, traditional methods to prepare CTP-derived porous graphene-like carbon materials normally need hard templates. This increases the manufacturing cost, and a lot of acid and water are used to remove the hard templates. Here, we adopt a facile coal tar pitch-blowing strategy using a novel blowing agent to synthesize an N, S co-doped porous graphene-like carbon (NSPC) material and employ it as the electrode material of supercapacitors. The porous property provides abundant active sites and short diffusion pathways for charge storage and transfer. The heteroatom doping not only accelerates charge transfer but also provides extra pseudo-capacitance [9]. Compared with single heteroatom doping that

* Corresponding authors at: School of Environmental and Chemical Engineering, Shenyang University of Technology, Shenyang 110870, China (Y. Wu). College of Chemistry and Chemical Engineering, Shihezi University, Shihezi 832003, China (G. Wang). Department of Chemistry, University College London, London WC1H 0AJ, UK (Y. Xu).

E-mail addresses: wanggang@shzu.edu.cn (G. Wang), yuhanwu@sut.edu.cn (Y. Wu), y.xu.1@ucl.ac.uk (Y. Xu).

https://doi.org/10.1016/j.cplett.2023.140712
Received 20 April 2023; Received in revised form 2 July 2023; Accepted 2 July 2023
Available online 4 July 2023

improves merely one aspect of performance, dual-doping can improve the overall performance of materials owing to the synergetic effect [10]. We take investigate its electrochemical properties as the electrode for supercapacitors. The capacitance of NSPC is 195.6 F g^{-1} at 1 A g^{-1}, and the retention is 95.22% after 10,000 cycles. To further improve the electrochemical performance, we activated NSPC with the chemical activator. The a-NSPC shows a high capacitance of 348 F g^{-1} at 1 A g^{-1} and good cycle stability with over 97.44% capacitance retention after 10,000 cycles. Although the electrochemical performance of NSPC was unsatisfactory, we would like to point out that NSPC just acted as an intermediate material to prepare a-NSPC, and a-NSPC exhibited excellent performance at all tested current densities (shown in Fig. 4e). To further demonstrate the excellent performance obtained, we have summarized the performance of similar carbon materials that have been reported in Table S1, and a-NSPC is one of the best among the reported carbon materials in recent years. Our work may provide a feasible way for the large-scale production of electrode materials with superior electrochemical performance and economic benefits.

2. Experimental section

CTP and $(NH_4)_2SO_4$ were mixed with a mass ratio of 1:5, and the mixture was pre-oxidized at 200 °C in air. Carbonization was conducted at an Ar atmosphere (50 mL min^{-1}) and heated for 2 h at a temperature sequence of 300, 500, and 1000 °C. The obtained black powders were labeled as NSPC. Afterward, NSPC was activated by KOH at 800 °C, namely a-NSPC. The direct carbonization CTP (DC-CTP) was prepared by the same condition without adding $(NH_4)_2SO_4$ and KOH. The properties of CTP and characterization information are given in Supporting Information.

3. Results and discussion

Fig. 1 illustrates the preparation procedure of NSPC and a-NSPC. $(NH_4)_2SO_4$ was used as a blowing gas source to produce a bubbly structure and well mixed with CTP via ball-milling. The mixture was first pre-oxidized at 200 °C in air, where CTP gradually hardened and reduce its fluidity. Subsequently, $(NH_4)_2SO_4$ decomposed into NH_3 and SO_2 during the high-temperature carbonization up to 1000 °C, and the released gases created thin-walled bubbles within the mixture. At the same time, NH_3 and SO_2 acted as the doping sources of N and S, hence forming an N and S co-doped carbon material with a porous graphene-like structure (NSPC) at the end of carbonization. Afterward, NSPC was further activated by KOH at 800 °C to increase BET-specific surface area and microscale pore content. Thermogravimetric (TG) was used to confirm the effect of $(NH_4)_2SO_4$ (Fig S1). The major thermal decomposition takes place at 250–450 °C, indicating that $(NH_4)_2SO_4$ was not decomposed by pre-oxidation treatment and plaid a foaming role in the subsequent carbonization process.

The morphology characterization of the samples was performed by field emission scanning electron microscopy (FESEM) and transmission electron microscopy (TEM). Both samples exhibit multi-porous structures with different sizes (Fig. 2a and b). The unique porous structure originated from the gases released from the decomposition of $(NH4)_2SO_4$ during the carbonization process. A close observation of the TEM images with a higher magnification reveals that NSPC features a great number of bubble-like structures with thin graphene layers in a diameter range of 50–100 nm (Fig. 2c and d). Notably, the unique structure was preserved after the KOH activation and a-NSPC possesses more porous compared with NSPC. The phenomenon of the interconnected 3D porous network could be beneficial for the fast ion transfer and the infiltration of electrolytes [11]. Owing to plenty of the materials are initially stored in the interconnected ion-buffering reservoirs and the few-layer graphene walls around them are covered by it, providing a quick supply and short diffusion distance [12]. The porous structures were further characterized using N_2 adsorption–desorption isotherms (Fig. 2e and f). As shown in Fig. 2e, both samples exhibited a sharply increased adsorption capacity at low relative pressures and an obvious hysteresis loop at a relative pressure between 0.5 and 1.0, indicating a similar micropore-dominated structure with a certain amount of mesopores [13]. a-NSPC had a higher N_2 adsorption capacity than NSPC, indicating that it possessed abundant micropores [14]. Generally, micropores ($\leq$2 nm) are beneficial for enhancing charge storage, and mesopores (2–50 nm) can facilitate ion transfer [15]. The results of the pore size distribution (Fig. 2f) confirm that both samples have a large number of micropores and mesopores, but a-NSPC possesses a higher micropores and mesopores pore volume. Meanwhile, the specific surface area of a-NSPC is over two times larger than that of NSPC (2326.3 vs. 1119.4 m^2 g^{-1}, Table S2), activation is conducive to the formation of micropores, which causes the increase of BET-specific surface area for the porous carbons. More micropores can provide sufficient active sites for redox reactions, and rich mesoporous/macroporous channels can shorten the distance of ion transport and facilitate electron/charge transfer [16]. Thus, the high specific surface area with reasonable pore size distribution is in favor of fast redox reaction and charge transfer [17,18].

The Raman spectra of both samples show the characteristic D-band at 1350 cm^{-1} and G-band at 1590 cm^{-1} (Fig. 3a). Notably, the I_D/I_G ratio of a-NSPC and NSPC are 1.12 and 1.11, respectively. The I_D/I_G ratio normally increases after KOH activation [19,20], but lower the content of heteroatom doping, which may cause the reduction of the I_D/I_G ratio [21,22]. Therefore, the slight change may be due to the KOH activation and the decrease of heteroatom doping level. As seen from the X-ray diffractometry (XRD) patterns (Fig. 3b), there are two humps centered around 23° and 43°. Similar results of a-NSPC and NSPC reveal the amorphous structure and preserved C frameworks after the KOH activation [23]. The X-ray photoelectron spectroscopy (XPS) survey spectra are shown in Fig. 3c. They clearly show C, N, S, and O elements (Fig. 3c), and the detailed element contents are summarized in Table S3 [24]. In DC-CTP, there are only a small amount of N and S elements (Fig. S2). As for NSPC and a-NSPC, during the KOH activation process, the reaction between C and KOH at a high temperature under an inert atmosphere is responsible for the micropores formed. The sharp decrease for the N and S heteroatoms content indicates these bonds of C atoms and heteroatoms were broken with the process of KOH activation [25]. In addition, a-NSPC showed a decrease of N and S contents while an increase in O content. It was caused by KOH corrosion. The introduction of heteroatom (N and S) could be helpful to increase the capacitance by reversible redox reactions and enhance electrode surface wettability [26]. And the appropriate and more proportion of oxygen groups (including C=O and

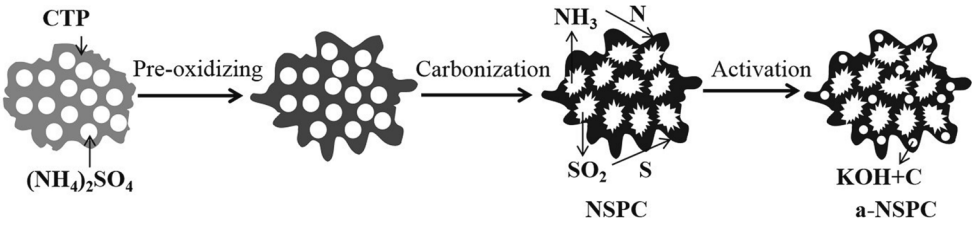

Fig. 1. Illustration of the synthetic process of NSPC and a-NSPC.

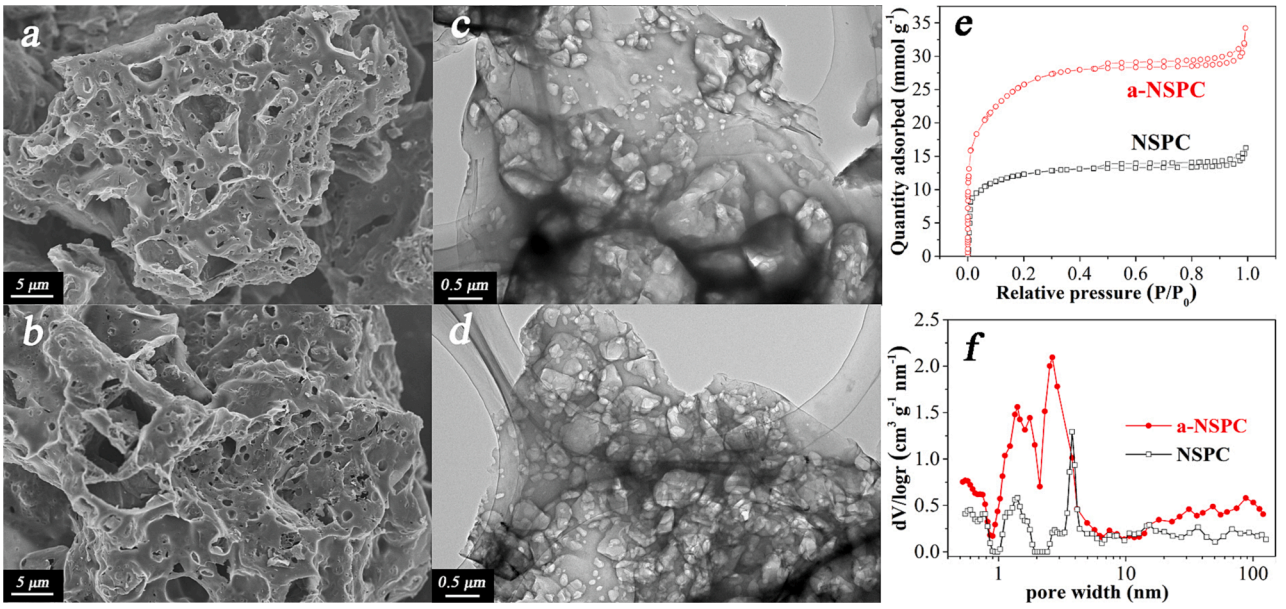

Fig. 2. (a–b) FESEM images, (c-d) TEM images, (e) and (f) N_2 adsorption–desorption isotherms and pore size distribution of NSPC (a and c) and a-NSPC (b and d).

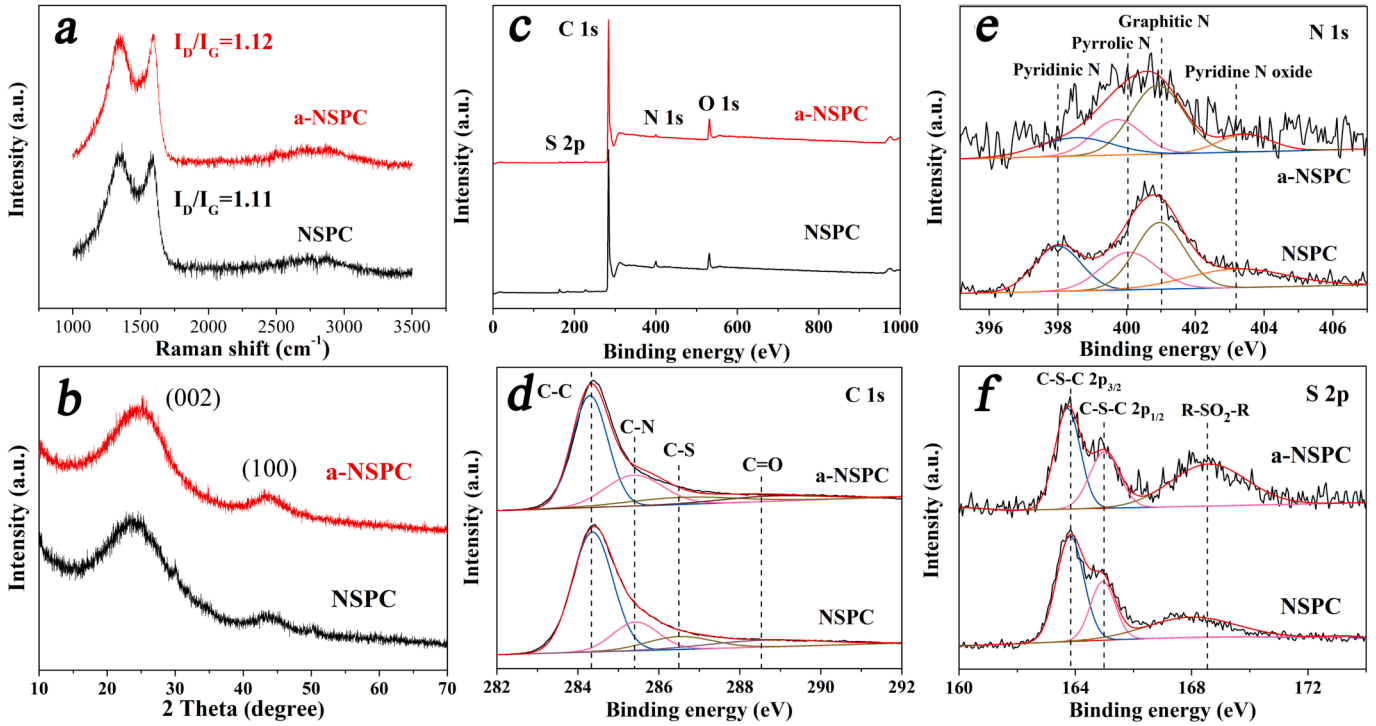

Fig. 3. (a) Raman spectra, (b) XRD patterns, (c) XPS survey spectra, (d) high-resolution C 1 s, (e) N 1 s, (f) S 2p spectra of NSPC and a-NSPC.

C–O) is beneficial for capacitance promotion [27]. The high-resolution C 1 s spectra of the samples (Fig. 3d) can be deconvoluted to four peaks at 284.4, 285.4, 286.6, and 288.6 eV, respectively, corresponding to C–C, C–N, C–S, and C=O bonds, respectively [28]. In high-resolution N 1 s spectra (Fig. 3e), four peaks can be attributed to pyridinic N (398.1 eV), pyrrolic N (400.3 eV), graphitic N (401.1 eV), and pyridine N oxide (403.2 eV) [29]. Interestingly, the pyridine N and pyrrolic N peaks are reduced after the activation by KOH, while the graphitic N peak is well maintained; these results illuminate that the C atoms around pyridinic-N and pyrrolic N species, mainly located at the defect sites caused by reactions with KOH, and give priority to form microporous structure [30]. These results also indicate that pyridine N and pyrrolic N are more active than graphitic N [31,32]. Fig. 3f shows high-resolution S 2p spectra, the peaks at 163.9 and 165.0 eV are related to thiophene S $2p_{3/2}$ and thiophene S $2p_{1/2}$ (such as C–S–C and C-S bridges). The band at 168.6 eV is attributed to oxidized S such as C-SO_x-C (x = 2, 3, or 4) [33]. After the activation by KOH, the content of oxidized S increased, but the specific value of thiophene S $2p_{3/2}$ and thiophene S $2p_{1/2}$ have not changed. This means the S atoms in neutral form were either consumed or altered into the oxidized sulfur during the KOH activation [32]. The XPS results confirm the incorporation of N and S into the C frameworks successfully and these heteroatoms still can be survived after the activation.

Cyclic voltammetry (CV) and galvanostatic charge/discharge (GCD) measurements were used to evaluate electrochemical performance

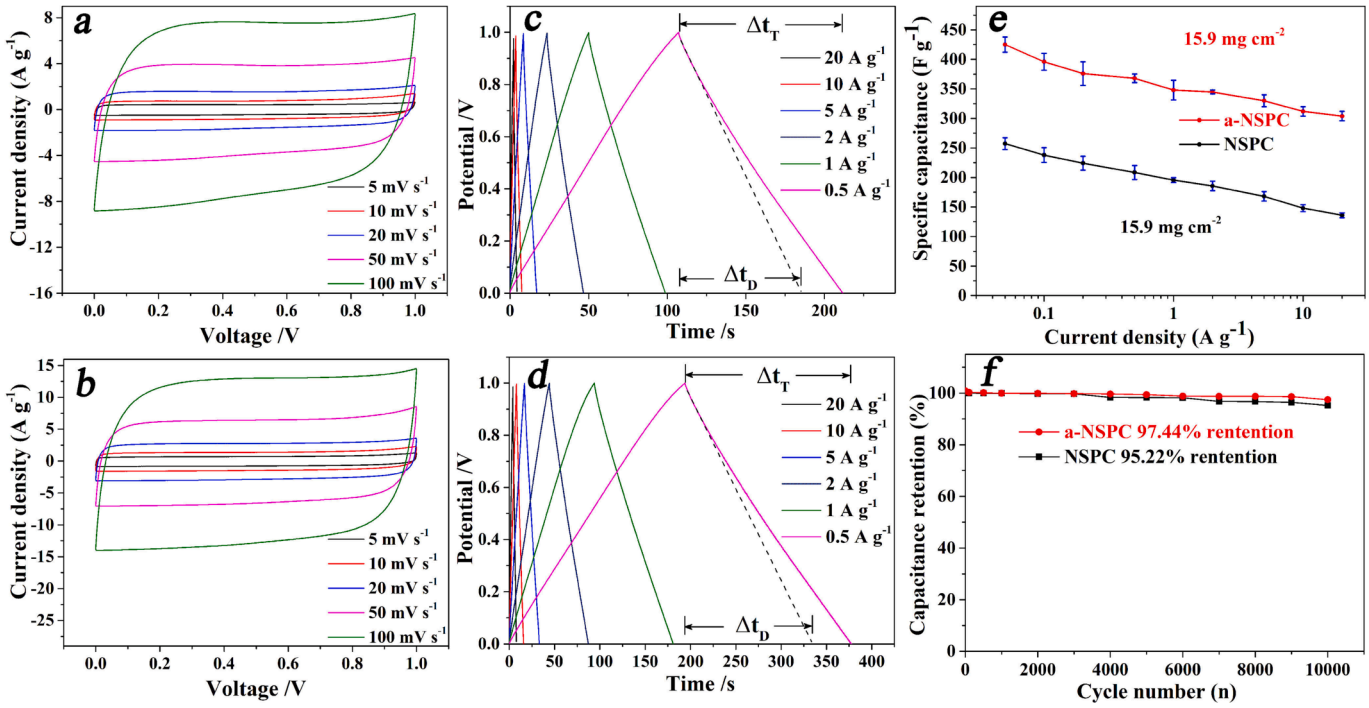

Fig. 4. (a–b) CV curves at various scan rates, (c-d) GCD curves at various current densities, (e) capacitance at different current densities, and (f) capacitance retention at 1 A g^{-1} of NSPC and a-NSPC electrodes.

(Fig. 4). Fig. 4a and 4b show the CV curves at different scan rates of 5, 10, 20, 50, and 100 mV s^{-1}. Their CV curves exhibit nearly quasi-rectangular shapes with bumps at 0 to 0.6 V, suggesting their combined capacitance from double-layer capacitance based on ion adsorption/desorption and pseudo-capacitance caused by redox reactions of doped functional groups [34]. And the CV curves of a-NSPC possess a larger area than the CV curves of NSPC owing to the desirable porous structure and large specific surface area of this sample, which suggests the high specific capacitance of a-NSPC. The shapes of the GCD curves are nearly symmetric triangular without a dramatic distortion at a current density range of 0.5–20 A g^{-1} (Fig. 4c and 4d), suggesting the capacitive nature of storing charges and the great electrochemical reversibility. These symmetric triangular shapes with a slight deviation, indicating that the overall capacitance is a mixture of pseudo-capacitance and electrochemical double-layer capacitance [35]. To calculate the pseudocapacitance, extended lines of the linear parts of the discharge curves have been drawn, which represent the double-layer capacitance parts of the discharge curves. Obviously, t_T is the total discharge time of the overall capacitance, and t_D is the discharge time of the double-layer capacitance type [36]. Thus, the percentages of pseudocapacitance of NSPC and a-NSPC at the current density of 0.5 A g^{-1} can be calculated to be 24.0 %, and 22.4 %, respectively. Their capacitances at different current densities are shown in Fig. 4e. Under the mass loading of 15.9 mg cm^{-2}, the capacitance of NSPC is 136 F g^{-1} at 20 A g^{-1}, being only 65.4% of low-rate capacitance at 0.5 F g^{-1}, while a-NSPC delivers 304 F g^{-1} at 20 A g^{-1}, and its retention is as high as 82.6%. More importantly, the electrode areal capacitances of NSPC and a-NSPC are 3.3 and 4.8 F cm^{-2} at 20 A g^{-1}, respectively. It may be owing to the well-developed mesoporous channels of a-NSPC are greatly beneficial to the charge storage and charge transfer, and the N, S-co-doping could also assist in the electrolyte wettability to the carbon surface, creating more active sites for highly efficient charge storage [37,38]. The prepared electrodes NSPC and a-NSPC exhibited energy densities of 8.94 and 14.76 W h kg^{-1}, respectively, at a power density of 50 W kg^{-1} (Fig. S3), showing great potential for practical applications [39]. Both NSPC and a-NSPC electrodes display great long-term cycling stability. After 10,000 successive charge–discharge cycles at 1 A g^{-1}, the capacitance retentions are 95.22% and 97.44% for NSPC and a-NSPC, respectively (Fig. 4f).

4. Conclusions

In this work, industrial byproduct CTP was utilized as a carbon precursor to synthesize an N, S co-doped graphene-like porous carbon via an ammonium sulfate-assisted chemical blowing strategy. Afterward, NSPC was activated by a chemical method to form a-NSPC with a high mesoscale pore content and a high surface area. Serving as electrode materials for supercapacitors, NSPC and a-NSPC exhibited capacitance of 208.6 and 368 F g^{-1} at 0.5 A g^{-1}, respectively. Under the mass loading of 15.9 mg cm^{-2}, the electrode areal capacitances of NSPC and a-NSPC are 3.3 and 4.8 F cm^{-2} at 20 A g^{-1}, respectively. More importantly, the capacitance retentions of NSPC and a-NSPC electrodes retained as high as 95.22% and 97.44%, respectively, at 1 A g^{-1} after 10,000 cycles. The low cost and great electrochemical performance endow them with strong competitiveness. Also, the facile preparation method may open up an avenue toward large-scale electrochemical energy storage applications.

CRediT authorship contribution statement

Gang Li: Methodology, Data curation, Writing – original draft. **Shanshan Chen:** Investigation. **Yonggang Wang:** Writing – review & editing. **Gang Wang:** Conceptualization. **Yuhan Wu:** Formal analysis, Writing – review & editing. **Yang Xu:** Conceptualization, Writing – review & editing.

Declaration of Competing Interest

The authors declare that they have no known competing financial interests or personal relationships that could have appeared to influence the work reported in this paper.

Data availability

Data will be made available on request.

Acknowledgements

G.W. acknowledges the support of the National Natural Science Foundation of China (NSFC) (21865025). Y.X. acknowledges the support of the Engineering and Physical Sciences Research Council (EP/V000152/1, EP/X000087/1) and Leverhulme Trust (RPG-2021-138). For the purpose of open access, the author has applied a Creative Commons Attribution (CC BY) licence to any Author Accepted Manuscript version arising.

Appendix A. Supplementary data

Supplementary data to this article can be found online at https://doi.org/10.1016/j.cplett.2023.140712.

References

[1] X. He, X. Xie, J. Wang, X. Ma, Y. Xie, J. Gu, N. Xiao, J. Qiu, From fluorene molecules to ultrathin carbon nanonets with an enhanced charge transfer capability for supercapacitors, Nanoscale 11 (2019) 6610–6619, https://doi.org/10.1039/c9nr00068b.
[2] Y. Yang, H. Niu, F. Qin, Z. Guo, J. Wang, G. Ni, P. Zuo, S. Qu, W. Shen, MnO2 doped carbon nanosheets prepared from coal tar pitch for advanced asymmetric supercapacitor, Electrochim. Acta 354 (2020) 136667, https://doi.org/10.1016/j.electacta.2020.136667.
[3] M. Li, W. Zhang, T. Liu, J. Mou, Y. Xu, J. Huang, M. Liu, Hierarchical hollow microspheres of carbon nanorods with enhanced supercapacitor performance, Mater. Today Commun. 28 (2021) 102500, https://doi.org/10.1016/j.mtcomm.2021.102500.
[4] F. Wei, X. He, H. Bi, S. Jiao, N. Xiao, J. Qiu, 3D hierarchical carbons composed of cross-linked porous carbon nanosheets for supercapacitors, J. Power Sources 474 (2020) 228698, https://doi.org/10.1016/j.jpowsour.2020.228698.
[5] X. Wang, Y. Zhang, C. Zhi, X.i. Wang, D. Tang, Y. Xu, Q. Weng, X. Jiang, M. Mitome, D. Golberg, Y. Bando, Three-dimensional strutted graphene grown by substrate-free sugar blowing for high-power-density supercapacitors, Nat. Commun. 4 (2013) 2905, https://doi.org/10.1038/ncomms3905.
[6] J. Zhou, S. Zhang, Y.-N. Zhou, W. Tang, J. Yang, C. Peng, Z. Guo, Biomass-derived carbon materials for high-performance supercapacitors: current status and perspective, Electrochem. Energy Rev. 4 (2021) 219–248, https://doi.org/10.1007/s41918-020-00090-3.
[7] Y. Wang, Q. Qu, S. Gao, G. Tang, K. Liu, S. He, C. Huang, Biomass derived carbon as binder-free electrode materials for supercapacitors, Carbon 155 (2019) 706–726, https://doi.org/10.1016/j.carbon.2019.09.018.
[8] X. He, H. Zhang, H. Zhang, X. Li, N. Xiao, J. Qiu, Direct synthesis of 3D hollow porous graphene balls from coal tar pitch for high performance supercapacitors, J. Mater. Chem. A 2 (2014) 19633–19640, https://doi.org/10.1039/c4ta03323j.
[9] G. Ni, F. Qin, Z. Guo, J. Wang, W. Shen, Nitrogen-doped asphaltene-based porous carbon fibers as supercapacitor electrode material with high specific capacitance, Electrochim. Acta 330 (2020)135270. https://doi.org/10.1016/j.electacta.2019.135270.
[10] Y. Li, G. Wang, T. Wei, Z. Fan, P. Yan, Nitrogen and sulfur co-doped porous carbon nanosheets derived from willow catkin for supercapacitors, Nano Energy 19 (2016) 165–175. https://doi.org/10.1016/j.nanoen.2015.10.038.
[11] L. Sun, Y. Gong, D. Li, C. Pan, Biomass-derived porous carbon materials: synthesis, designing, and applications for supercapacitors, Green Chem 24 (2022) 3864–3894. https://doi.org/10.1039/d2gc00099g.
[12] Y. Li, Z. Li, P.K. Shen, Simultaneous formation of ultrahigh surface area and three-dimensional hierarchical porous graphene-like networks for fast and highly stable supercapacitors, Adv. Mater. 25 (2013) 2474–2480. https://doi.org/10.1002/adma.201205332.
[13] Y. Jiang, Z. Jiang, M. Shi, Z. Liu, S. Liang, J. Feng, R. Sheng, S. Zhang, T. Wei, Z. Fan, Enabling high surface and space utilization of activated carbon for supercapacitors by homogeneous activation, Carbon 182 (2021) 559–563. https://doi.org/10.1016/j.carbon.2021.06.039.
[14] X. Meng, Q. Cao, Li'e Jin, X. Zhang, S. Gong, P. Li, Carbon electrode materials for supercapacitors obtained by co-carbonization of coal-tar pitch and sawdust, J. Mater. Sci. 52 (2017) 760–769, https://doi.org/10.1007/s10853-016-0370-1.
[15] H. Liu, W. Shi, H. Song, Y. Chang, L. Feng, W. Hou, Y. Li, Y. Zhao, S. Zhu, G. Han, Dual-role salt-assisted construction of hierarchically porous carbon for supercapacitors with high energy and power density, ACS Appl. Energy Mater. 6 (2023) 222–232, https://doi.org/10.1021/acsaem.2c02807.
[16] W. Feng, F. Zhang, K. Wei, B. Zhai, C. Yu, Controlled synthesis of porous carbons and their electrochemical performance for supercapacitors, Chem. Phy. Lett. 806 (2022) 140066. https://doi.org/10.1016/j.cplett.2022.140066.
[17] X. Zhao, C. Li, L. Sha, K. Yang, M. Gao, H. Chen, J. Jiang, In-built fabrication of MOF assimilated porous hollow carbon from pre-hydrolysate for supercapacitor, Polymers 14 (2022) 3377. https://doi.org/10.3390/polym14163377.
[18] H. Liu, H. Song, W. Hou, Y. Chang, Y. Zhang, Y. Li, Y. Zhao, G. Han, Coal tar pitch-based hierarchical porous carbons prepared in molten salt for supercapacitors, Mater. Chem. and Phys. 265 (2021) 124491, https://doi.org/10.1016/j.matchemphys.2021.124491.
[19] W. Geng, F. Ma, G. Wu, S. Song, J. Wan, D. Ma, MgO-templated hierarchical porous carbon sheets derived from coal tar pitch for supercapacitors, Electrochim. Acta 191 (2016) 854–863. https://doi.org/10.1016/j.electacta.2016.01.148.
[20] W. Deng, T. Kang, H. Liu, J. Zhang, N. Wang, N. Lu, Y. Ma, A. Umar, Z. Guo, Potassium hydroxide activated and nitrogen doped graphene with enhanced supercapacitive behavior, Sci. Adv. Mater. 10 (2018) 937–949. https://doi.org/10.1166/sam.2018.3279.
[21] J. Deng, Z. Peng, Z. Xiao, S. Song, H. Dai, L. Li, Porous doped carbons from anthracite for high-performance supercapacitors, Appl. Sci. 10 (2020) 1081. https://doi.org/10.3390/app10031081.
[22] M.R. Pallavolu, S. Prabhu, R.R. Nallapureddy, A.S. Kumar, A.N. Banerjee, S.W. Joo, Bio-derived graphitic carbon quantum dot encapsulated S- and N-doped graphene sheets with unusual battery-type behavior for high-performance supercapacitor, Carbon 202 (2023) 93–102. https://doi.org/10.1016/j.carbon.2022.10.077.
[23] J. Liu, Y. Deng, X. Li, L. Wang, Promising nitrogen-rich porous carbons derived from one-step calcium chloride activation of biomass-based waste for high performance supercapacitors, ACS Sustainable Chem. Eng. 4 (2016) 177–178. https://doi.org/10.1021/acssuschemeng.5b00926.
[24] G. Zhang, T. Guan, J. Qiao, J. Wang, K. Li, Free-radical-initiated strategy aiming for pitch-based dual-doped carbon nanosheets engaged into high-energy asymmetric supercapacitors, Energy Storage Mater 26 (2020) 119–128. https://doi.org/10.1016/j.ensm.2019.12.038.
[25] M. Sevilla, R. Mokaya, Energy storage applications of activated carbons: supercapacitors and hydrogen storage, Energy Environ. Sci. 7 (2014) 1250–1280. https://doi.org/10.1039/c3ee43525c.
[26] H. Liu, X. Yao, H. Song, W. Hou, Y. Chang, Y. Zhang, S. Zhu, Y. Li, Y. Zhao, G. Han, Molten salt-confined construction of nitrogen-doped hierarchical porous carbon for high-performance supercapacitors, Diamond Related Mater. 128 (2022) 109289, https://doi.org/10.1016/j.diamond.2022.109289.
[27] F. Razmjooei, K. Singh, T.H. Kang, N. Chaudhari, J. Yuan, J.S. Yu, Urine to highly porous heteroatom-doped carbons for supercapacitor: a value added journey for human waste, Sci. Rep. 7 (2017) 10910. https://doi.org/10.1038/s41598-017-11229-6.
[28] J.G. Wang, H. Liu, X. Zhang, M. Shao, B. Wei, Elaborate construction of N/S-co-doped carbon nanobowls for ultrahigh-power supercapacitors, J. Mater. Chem. A 6 (2018) 17653–17661. https://doi.org/10.1039/c8ta07573e.
[29] R. Li, L. Lai, S. Su, H. Dai, Y. Cui, X. Zhu, One-step facile hydrothermal synthesis of heteroatom-doped porous graphene reduced comparatively by different reductants for high performance supercapacitors, Mater, Today Commun 23 (2020) 101128. https://doi.org/10.1016/j.mtcomm.2020.101128.
[30] D. Zhang, M. Han, B. Wang, Y. Li, L. Lei, K. Wang, Y.i. Wang, L. Zhang, H. Feng, Superior supercapacitors based on nitrogen and sulfur co-doped hierarchical porous carbon: excellent rate capability and cycle stability, J. Power Sources 358 (2017) 112–120, https://doi.org/10.1016/j.jpowsour.2017.05.031.
[31] Y. Cao, G. Ning, C. Xu, X. Huang, Y. Yu, W. Li, C. Xu, Selective activation of S or N-containing carbon segments by alkalic or acidic activators, Ind. Eng. Chem. Res. 58 (2019) 9048–9055, https://doi.org/10.1021/acs.iecr.9b00306.
[32] C. Ma, T. Lu, J. Shao, J. Huang, X. Hu, L. Wang, Biomass derived nitrogen and sulfur co-doped porous carbons for efficient CO2 adsorption, Sep. Purif. Technol. 281 (2022) 119899. https://doi.org/10.1016/j.seppur.2021.119899.
[33] G. Chao, L. Zhang, D. Wang, S. Chen, H. Guo, K. Xu, W. Fan, T. Liu, Activation of graphitic nitrogen sites for boosting oxygen reduction, Carbon 159 (2020) 611–616. https://doi.org/10.1016/j.carbon.2019.12.052.
[34] T. Guan, K. Li, J. Zhao, R. Zhao, G. Zhang, D. Zhang, J. Wang, Template-free preparation of layer-stacked hierarchical porous carbons from coal tar pitch for high performance all-solid-state supercapacitors, J. Mater. Chem. A 5 (2017) 15869–15878, https://doi.org/10.1039/c7ta02966g.
[35] C. Chen, M. Zhao, Y. Cai, G. Zhao, Y. Xie, L.i. Zhang, G. Zhu, L. Pan, Scalable synthesis of strutted nitrogen doped hierarchical porous carbon nanosheets for supercapacitors with both high gravimetric and volumetric performances, Carbon 179 (2021) 458–468, https://doi.org/10.1016/j.carbon.2021.04.062.
[36] Y. Tan, C. Xu, G. Chen, Z. Liu, M. Ma, Q. Xie, N. Zheng, S. Yao, Synthesis of ultrathin nitrogen-doped graphitic carbon nanocages as advanced electrode materials for supercapacitor, ACS Appl. Mater. Interfaces 5 (2013) 2241–2248, https://doi.org/10.1021/am400001g.
[37] C. Shao, L. Wu, H. Zhang, Q. Jiang, X. Xu, Y. Wang, S. Zhuang, H. Chu, L. Sun, J. Ye, B. Li, X. Wang, A versatile approach to boost oxygen reduction of Fe-N-4 sites by controllably incorporating sulfur functionality, Adv. Funct. Mater. 31 (2021) 2100833. https://doi.org/10.1002/adfm.202100833.
[38] F. Wu, M. Liu, Y. Li, X. Feng, K. Zhang, Y. Bai, X. Wang, C. Wu, High-mass-loading electrodes for advanced secondary batteries and supercapacitors, Electrochem. Energy Rev. 4 (2021) 382–446. https://doi.org/10.1007/s41918-020-00093-0.
[39] W. Tian, J. Zhu, Y. Dong, J. Zhao, J. Li, N. Guo, H. Lin, S. Zhang, D. Jia, Micelle-induced assembly of graphene quantum dots into conductive porous carbon for high rate supercapacitor electrodes at high mass loadings, Carbon 161 (2020) 89–96. https://doi.org/10.1016/j.carbon.2020.01.044.